

[N II] fine-structure emission at 122 and 205 μm in a galaxy at $z=2.6$: a globally dense star-forming interstellar medium

M. J. DOHERTY ¹, J. E. GEACH ¹, R. J. IVISON ² AND S. DYE ³

¹Centre for Astrophysics Research, Department of Physics, Astronomy & Mathematics, University of Hertfordshire, College Lane, Hatfield AL10 9AB, UK

²European Southern Observatory, Karl-Schwarzschild-Straße 2, D-85748 Garching, Germany

³School of Physics and Astronomy, University of Nottingham, University Park, Nottingham NG7 2RD, UK

ABSTRACT

We present new observations with the Atacama Large Millimeter/sub-millimeter Array of the 122- and 205- μm fine-structure line emission of singly-ionised nitrogen in a strongly lensed starburst galaxy at $z = 2.6$. The 122-/205- μm [N II] line ratio is sensitive to electron density, n_e , in the ionised interstellar medium, and we use this to measure $n_e \approx 300 \text{ cm}^{-3}$ averaged across the galaxy. This is over an order of magnitude higher than the Milky Way average, but comparable to localised Galactic star-forming regions. Combined with observations of the atomic carbon (C I(1–0)) and carbon monoxide (CO $J = 4-3$) in the same system, we reveal the conditions in this intensely star-forming system. The majority of the molecular interstellar medium has been driven to high density, and the resultant conflagration of star formation produces a correspondingly dense ionised phase, presumably co-located with myriad H II regions that litter the gas-rich disk.

1. INTRODUCTION

With the discovery of a population of high-redshift submillimeter-selected galaxies (SMGs) over two decades ago (Smail et al. 1997; Barger et al. 1998; Hughes et al. 1998), it became clear that some galaxies undergo episodes of intense star formation in the early Universe, with rates $1000\times$ that of the Milky Way. Thought to be the progenitors of the most massive galaxies in the Universe today (Simpson et al. 2014; Toft et al. 2014), undergoing a period of rapid assembly, a central question has been how such extreme levels of star formation are driven in these galaxies?

With the advent of sensitive, resolved submillimeter and millimeter imaging and spectroscopy of the SMG population at high redshift (see Hodge & da Cunha 2020, for a recent review), a broad picture is emerging: molecular gas reservoirs are extended on scales of several kiloparsecs (Menéndez-Delmestre et al. 2009; Ivison et al. 2011; Riechers et al. 2011) with a large fraction of the molecular interstellar medium (ISM) driven to high density, driving high instantaneous star-formation rates (SFRs) due to the increased fraction of the ISM participating in star formation at any one time (Gao & Solomon 2004; Oteo et al. 2017).

But what is the nature of star formation in these extreme systems? Is it essentially identical to what we observe in

discrete pockets in the disk of the Milky Way, but occurring more prevalently throughout the ISM? Or is the phenomenon of star formation in these extreme, early systems fundamentally different — perhaps due to systematic differences in metallicity, stellar initial mass function, pressure, magnetic fields, and so-on? Ideally, one would like to understand the internal conditions in more detail: the density and phase structure, chemistry and physical distribution of the gas in high-redshift SMGs, where we use the label ‘SMG’ to broadly capture extreme star-forming galaxies.

Most progress to date has been in the exploitation of strongly gravitationally lensed systems (e.g. Koopmans et al. 2006; Swinbank et al. 2010; Conley et al. 2011; Wardlow et al. 2013; Dye et al. 2015; Dessauges-Zavadsky et al. 2019; Rybak et al. 2020). For example, SMMJ2135–0102 ($z = 2.3$), the so-called ‘Cosmic Eyelash’ (Swinbank et al. 2010) is one of the most comprehensively studied SMGs to date, and has provided valuable insights into the conditions of the ISM in a galaxy with an SFR roughly $100\times$ that of the Milky Way, close to the peak epoch of galaxy growth (e.g. Ivison et al. 2010; Thomson et al. 2012; George et al. 2014).

Danielson et al. (2011, 2013) showed that the cold molecular gas associated with star formation in the Cosmic Eyelash is exposed to UV radiation fields up to three orders of magnitude more intense than that of the Solar neighbourhood, with the star-forming molecular gas having a characteristic density of 10^4 cm^{-3} , similar to values seen in local ultraluminous infrared galaxies (Davies et al. 2003). Recent work on an-

other well studied lensed system, SDP 81 (Rybak et al. 2020), also suggests that a large fraction of the molecular ISM has been driven to high density, with star-formation occurring throughout the galaxy, but localised in dense star-forming complexes of size ~ 200 pc with conditions comparable to the Orion Trapezium cluster in the Milky Way (see also Swinbank et al. 2015). We note, however, that the interpretation of ‘clumps’ detected in high resolution interferometric imaging needs to be treated with caution, with Ivison et al. (2020) demonstrating that previously reported star-forming clumps in the Cosmic Eyelash are in fact spurious artifacts, a result of over-cleaning of relatively low signal-to-noise data.

Targets like the Cosmic Eyelash and SDP 81 are valuable because their lens-amplified flux offers a route to measure diagnostic tracers of the ISM and its conditions in a way that would be impossible in the unlensed case. These targets are, however, intrinsically rare. Here we focus on another strongly lensed SMG: ‘9io9’ (Geach et al. 2015). 9io9 is a galaxy discovered as part of the citizen science project *Spacewarps* (see Marshall et al. 2016; More et al. 2016) and independently as a bright millimetre source by *Planck* (Harrington et al. 2016), *Herschel* (Viero et al. 2014), and the Atacama Cosmology Telescope (Su et al. 2017). 9io9 lies at $z = 2.6$, close to the peak epoch of galaxy growth (Geach et al. 2018). Even after taking into account the $15\times$ magnification factor, 9io9 appears to have a total infrared luminosity, L_{IR} , exceeding $10^{13} L_{\odot}$, putting in the hyperluminous class, with an inferred SFR of around $2000 M_{\odot} \text{yr}^{-1}$, *modulo* the sometimes high and often hidden AGN contribution to L_{IR} in such systems (e.g. Ivison et al. 2019), and also *modulo* evidence suggesting that the stellar initial mass function in high-density star-forming regions is markedly top heavy (e.g. Romano et al. 2017; Zhang et al. 2018; Motte et al. 2018; Schneider et al. 2018; Brown & Wilson 2019, cf. Romano et al. 2019). It is therefore an excellent laboratory for studying the conditions of intense star formation in the early Universe.

In this paper we present new observations of 9io9 with the Atacama Large Millimeter/sub-millimeter Array (ALMA), building on the work of Geach et al. (2018). This study focuses on the [N II] 122- and 205- μm fine-structure lines. These lines trace the cool, ionised ISM (Goldsmith et al. 2015), and together can be used to constrain the electron density (e.g. Zhang et al. 2018, and references therein). With previous ALMA CO $J(4\rightarrow 3)$ and C I (1–0) observations (Geach et al. 2018) this allows us to link the properties of the dense molecular and the ionised phases of the ISM on identical scales in 9io9. In Section 2 we describe the observations and data reduction, in Section 3 we present our analysis, in Section 4 we interpret and discuss the main results of the analysis and present our conclusions in Section 5. Throughout we assume a ‘Planck 2015’ cosmology where

$H_0 = 68 \text{ km s}^{-1} \text{ Mpc}^{-1}$ and $\Omega_{\text{m}} = 0.31$ (Planck Collaboration et al. 2016).

2. OBSERVATIONS

9io9 (02^h09^m41^s.3, 00°15′58″.5, $z = 2.5543$) was observed with the ALMA 12-m array in project 2017.1.00814.S in Bands 4, 8 and 9. The details of the Band 4 observations are presented in Geach et al. (2018), and here we present the new Band 8 and 9 data. The Band 8 observations were conducted on 2018 August 26 and 2018 September 07 in two 40-min execution blocks with a representative frequency of approximately 411.5 GHz. The antenna configuration was C43–4 (with 47 antennas), with a maximum baseline of 783 m. The central frequencies of the four spectral windows were 397.466, 399.404, 409.481 and 411.481 GHz, designed to cover the the redshifted [N II] $^3P_1 \rightarrow ^3P_0$ fine-structure line ($\nu_{\text{rest}} = 1461.131$ GHz) and continuum emission. Calibrators included J0217+0144, J0423–0120 and J2253+1608. In two executions the total on-source integration time was 42 min, with an average precipitable water vapor column of 0.73 mm, resulting in an r.m.s. noise of 3 mJy beam^{-1} in a 15.6-MHz channel.

The Band 9 observations were conducted on 2018 August 19 in a single 70-min execution block. The antenna configuration was C43–3 (with 46 antennas), with a maximum baseline of 484 m. The representative frequency was approximately 692.3 GHz with eight spectral windows at 670.311, 672.249, 674.249, 676.202, 686.248, 688.201, 690.200 and 692.138 GHz. The Band 9 observations were designed to contain the redshifted [N II] $^3P_2 \rightarrow ^3P_1$ fine-structure line ($\nu_{\text{rest}} = 2459.380$ GHz) and continuum emission. Calibrators included J0217+0144 and J0522–3627. The total time on-source was 31 min, with an average precipitable water vapor column of 0.45 mm, resulting in an r.m.s. noise of 10 mJy beam^{-1} in a 15.6-MHz channel.

For the Band 8 data we used the pipeline-restored calibrated measurement set. For the Band 9 observations, due to unstable phases in two antennas (DA64 and DA24) we re-calibrated manually, flagging both dishes within the pipeline script. We imaged and cleaned the data using the CASA (v.5.1.0-74.e17) task, `tclean`. As in Geach et al. (2018), we employ multi-scale cleaning (at scales of $0''$, $0.5''$, and $1.25''$). First we produce dirty cubes to establish the r.m.s. (1σ) noise per channel, and then clean down to a threshold of 3σ . With natural weighting, the synthesised beams were $0.43'' \times 0.35''$ (FWHM, position angle 33°) and $0.32'' \times 0.28''$ (position angle 74°) in Bands 8 and 9, respectively. In order to produce data cubes that have closely matched resolution across Band 4, 8 and 9, we also produce *uv*-tapered maps with a scale of $0.6''$ noting that the *uv* plane is well sampled across all bands such that we expect negligible losses to extended emission on the scale of the lens

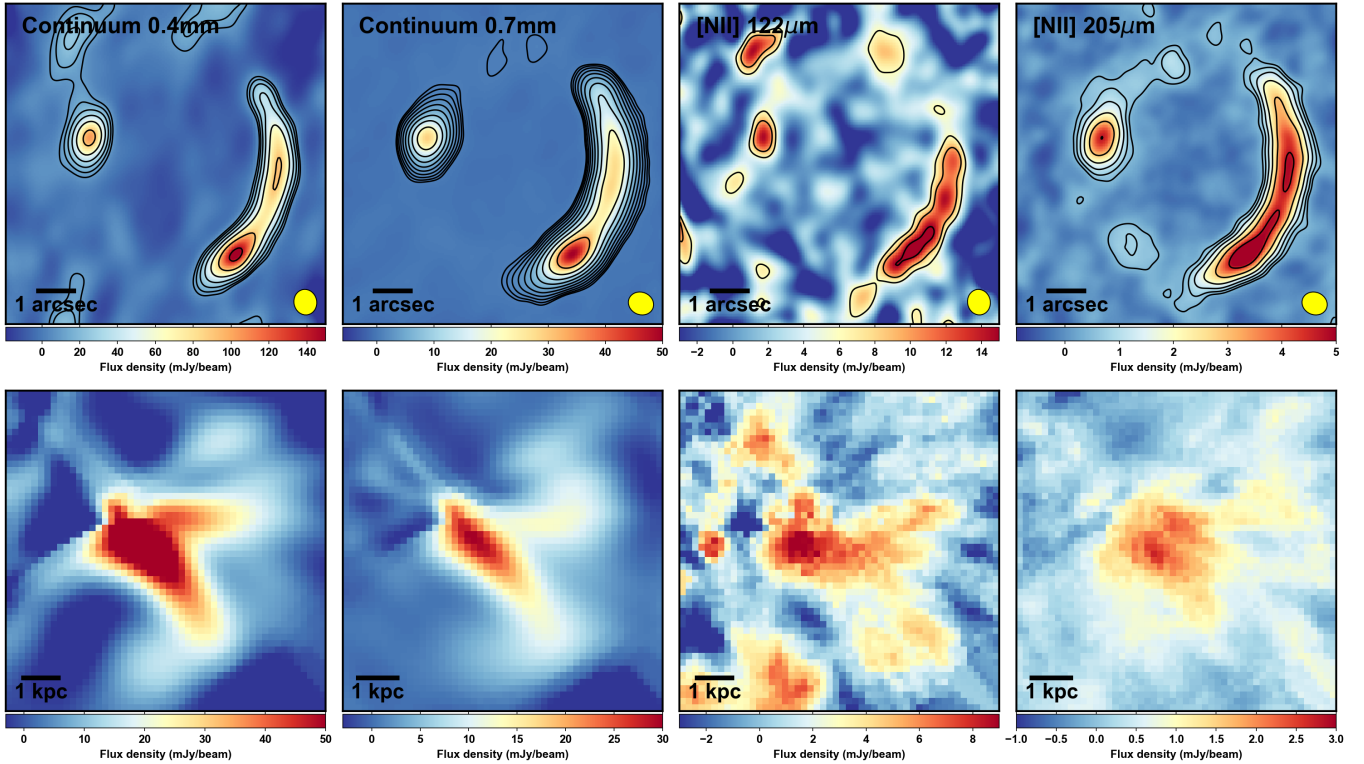


Figure 1. ALMA observations of 9io9. Top panels show the continuum at 0.4 and 0.7 mm and the continuum-subtracted [N II] 122- and 205- μm line emission, respectively, in the image plane, lower panels show the corresponding emission in the source plane. Contours in the image plane images are at logarithmically spaced (0.2 dex) intervals of σ , starting at 3σ .

(LAS $\lesssim 3\text{--}4''$). In Fig. 1 we present the image-plane maps of the line-free Band 8 (400 GHz) and Band 9 (680 GHz) continuum emission and the line-averaged [N II] $^3P_1 \rightarrow ^3P_0$ and $^3P_2 \rightarrow ^3P_1$ continuum-subtracted emission.

3. ANALYSIS

3.1. Lens model

We adopt the same lens model as Geach et al. (2018). Briefly, the lens model includes the gravitational potential of both the primary lensing galaxy ($z \approx 0.2$) and its smaller northern companion (assumed to be at the same redshift). The model uses the semi-linear inversion method of Warren & Dye (2003) to reconstruct the source plane surface brightness that best matches the observed Einstein ring for a given lens model. This process is iterated, varying the lens model and creating a source reconstruction at each iteration, until the global best fit lens model is found (Geach et al. 2018). The best fit model was used to produce source-plane cubes. Each slice was reconstructed with 50 realisations of a randomised Voronoi source plane grid (see Dye et al. 2018, for further details) and the mean taken, weighted by the log of the likelihood of each realisation. In Fig. 1 we show the equivalent continuum and line maps in the source plane. The resulting source plane reconstruction has an average beam size of 280 mas (FWHM) corresponding to a physical scale of

2.3 kpc in the source plane. Fig. 1 shows the source-plane images of the line-free Band 8 (400 GHz) and Band 9 (680 GHz) continuum emission and the line-averaged [N II] $^3P_1 \rightarrow ^3P_0$ and $^3P_2 \rightarrow ^3P_1$ continuum-subtracted emission. As can be seen in Figure 1, the [N II] 122 μm line measured in Band 9 appears to have an additional clump of emission to the NE not clearly visible (however detected) in the 205 μm map. This feature is multiply imaged in the image plane and also detected in the Band 8 data, so although at low significance unlikely to be spurious. However due to a lack of a continuum detection and the low significance of the detection, the strength of the 122 μm line in this region is unreliable. There are several other low significance features that do correlate with emission in other bands along the ring, but due to the relatively low signal-to-noise of the 122 μm line we do not attempt to interpret the resolved properties of the line itself, or the line ratio, concentrating our analysis on the integrated properties. Of course, with the 122 μm line strength now constrained, future observations could be obtained to address the resolved properties at higher signal-to-noise. Fig. 2 shows the [N II] doublet as well as the C I (1–0) and CO $J(4 \rightarrow 3)$ lines, scaled for comparison. In the following, all analysis is performed in the source plane. The errors quoted for the intrinsic source properties do not include any systematic un-

certainty introduced by the prescribed parametric lens model (see e.g. Schneider & Sluse 2013).

3.2. Line and continuum measurements

As we have resolved the global thermal dust continuum emission from 9io9 at high signal-to-noise in each of ALMA Bands 4, 8 and 9, with Band 9 probing close to the redshifted peak of the thermal emission, we can estimate L_{IR} (rest-frame 8–1000 μm) for the source, fully taking into account the effects of differential lensing since L_{IR} can be determined in the source plane. We fit the observed emission with a single-temperature modified blackbody spectrum, allowing the dust emissivity (β), dust temperature (T_{d}) and normalisation to be free parameters. Summing the luminosity within the region bound by the $\geq 3\sigma$ contour (in Band 8) we measure a total $L_{\text{IR}} = (1.1 \pm 0.2) \times 10^{13} L_{\odot}$. Thus, 9io9 is a hyperluminous infrared-luminous galaxy (HyLIRG) at $z \approx 2.6$. For reference, the total Band 8 and Band 9 source plane continuum flux densities are 12 mJy and 43 mJy at observed frequencies of 400 and 680 GHz, respectively.

We evaluate line luminosities using the standard relation Solomon et al. (1997)

$$\frac{L}{L_{\odot}} = \left(\frac{1.04 \times 10^{-3} \nu_{\text{obs}}}{\text{GHz}} \right) \left(\frac{D_{\text{L}}}{\text{Mpc}} \right)^2 \left(\frac{S\Delta V}{\text{Jy km s}^{-1}} \right) \quad (1)$$

where D_{L} is the luminosity distance, ν_{obs} is the observed frequency and $S\Delta V$ is the velocity-integrated line flux. Subtracting the continuum model from each pixel based on a linear fit to line free regions of the lines corresponding data cube allowing the gradient and normalisation vary as free parameters, the integrated flux density (measured within the same 3σ region as the continuum) of the [N II] 205- μm line is $S\Delta V = (2.37 \pm 0.06) \text{ Jy km s}^{-1}$, corresponding to $L_{205} = (4.7 \pm 0.1) \times 10^8 L_{\odot}$. For the [N II] 122- μm line, the integrated flux density is $S\Delta V = (7.6 \pm 0.9) \text{ Jy km s}^{-1}$, corresponding to $L_{122} = (2.6 \pm 0.3) \times 10^9 L_{\odot}$, integrating between -500 km s^{-1} and 300 km s^{-1} due to the [N II] lines being incomplete. By comparing to the CO $J(4 \rightarrow 3)$ and C I (1–0) lines we estimate we are missing $\approx 10\%$ of the total line flux for both lines, however this should not alter the resultant [N II] ratio as both lines are equally affected. Uncertainties are determined by adding Gaussian noise to each channel, with a scale determined from off-source regions of the datacube, taking the standard deviation of the pixel-to-pixel channel noise and scaling by the solid angle subtended by the 3σ mask used to define the total emission. Repeating this 1000 times and integrating the lines for each realisation allows us to estimate the uncertainties.

3.3. Electron density

With an ionisation potential of 14.5 eV, N^+ originates exclusively from the ionised ISM. N^+ thus traces H II regions

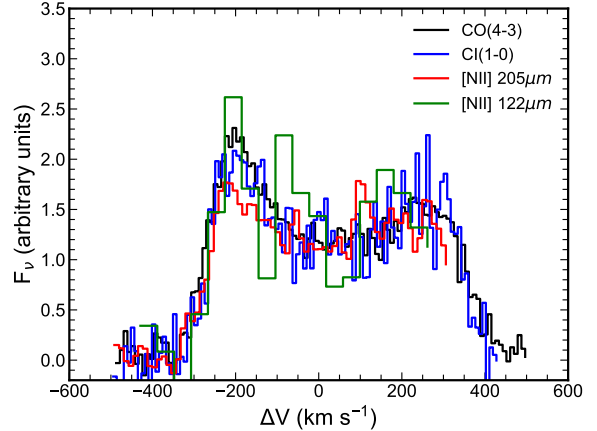


Figure 2. [N II] doublet, C I (1–0) and CO $J(4 \rightarrow 3)$, scaled such that each line has a common mean (on an arbitrary scale). All lines share a very similar double horned profile, indicating that the molecular and ionized phases are broadly tracing the same structures.

and is a good tracer of massive star formation, with its emission being directly related to the ionising photon rate and thus the number of massive stars (Zhao et al. 2016; Herrera-Camus et al. 2016). At lower densities ($0.01 \leq n_e \leq 0.1 \text{ cm}^{-3}$), N^+ is also a coolant of the warm ionised medium (WIM).

N^+ has three fine-structure levels: $^3P_{0,1,2}$. These are simply referred to as 0, 1, 2 in the following. If electron collisions are the primary excitation mechanism, we can write the collision rates as $C_{ij} = R_{ij}n_e$ where R_{ij} is the collision rate coefficient and n_e is the electron density. Following Goldsmith et al. (2015), the rate equations can be written

$$\begin{aligned} -(A_{21} + C_{21} + C_{20})n_2 + C_{12}n_1 + C_{02}n_0 &= 0 \\ (A_{21} + C_{21})n_2 - (A_{10} + C_{10} + C_{12})n_1 + C_{01}n_0 &= 0 \\ C_{20}n_2 + (A_{10} + C_{10})n_1 - (C_{02} + C_{01})n_0 &= 0 \end{aligned} \quad (2)$$

where n_0 , n_1 , and n_2 are the populations of each level, such that $n_0 + n_1 + n_2 = n(\text{N}^+)$, and A_{ij} are the Einstein coefficients. The 122- and 205- μm emission lines correspond to energy transitions E_{21} and E_{10} , respectively. For optically thin emission these are related to the line intensity of the $i \rightarrow j$ transition as

$$I_{ij} = \frac{A_{ij}E_{ij}N_i}{4\pi}, \quad (3)$$

where N_i is the column density of the upper level. The ratio of the line intensities then becomes

$$R = \frac{I_{21}}{I_{10}} = \frac{A_{21}E_{21}n_2}{A_{10}E_{10}n_1}, \quad (4)$$

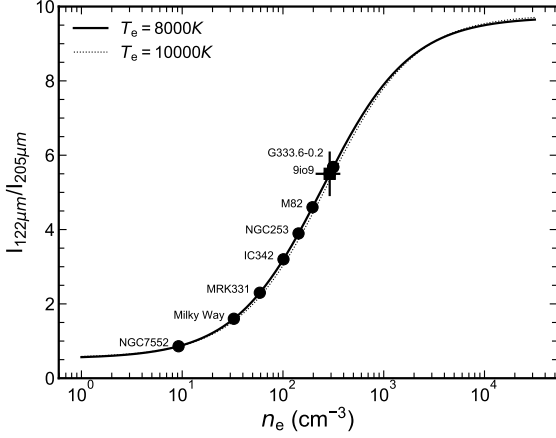


Figure 3. Derived electron density versus [N II] line ratio, including literature values found for a variety of Galactic and extragalactic sources. Note the insensitivity of n_e to the assumed electron temperature.

assuming the ratio of column densities equals the ratio of volume densities. The rate equations (2) yield

$$\frac{n_2}{n_1} = \frac{C_{12}(C_{01} + C_{02}) + C_{02}(A_{10} + C_{10})}{(A_{21} + C_{21} + C_{20})(A_{10} + C_{10}) + C_{20}C_{12}}. \quad (5)$$

Using $C_{ij} = R_{ij}n_e$, we derive a relation for the electron density which can be written in the form

$$n_e = \frac{d R - R_{\min}}{c R_{\max} - R}, \quad (6)$$

where

$$\begin{aligned} a &= R_{12}R_{01} + R_{02}R_{10} + R_{02}R_{12} \\ b &= R_{02}A_{10} \\ c &= R_{02}R_{21} + R_{01}R_{21} + R_{01}R_{12} \\ d &= A_{21}(R_{02} + R_{01}) \\ R_{\min} &= \frac{A_{21}E_{21} b}{A_{10}E_{10} d} \\ R_{\max} &= \frac{A_{21}E_{21} a}{A_{10}E_{10} c}. \end{aligned} \quad (7)$$

Using collision rates from [Tayal \(2011\)](#) for a kinetic temperature, $T_e = 8000$ K, and assuming that collision rates are independent of temperature¹ yields an expression for the electron density based on the line ratios:

$$n_e = 247 \left(\frac{R - 0.52}{9.73 - R} \right) \text{cm}^{-3}. \quad (8)$$

¹ Although the relation is not completely temperature independent, the derived electron density does not vary by more than 10% for a 2000 K increase in kinetic temperature, as can be seen in Fig. 3.

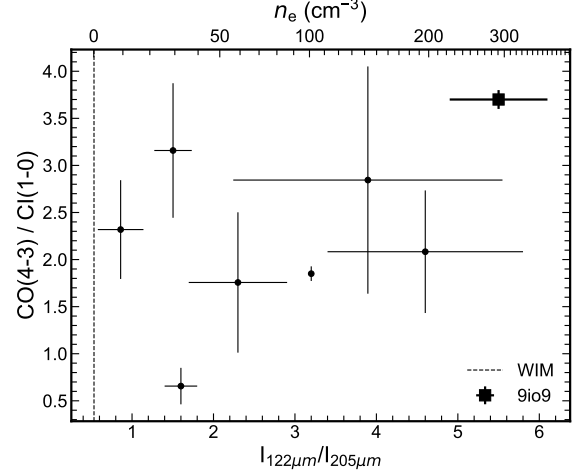


Figure 4. [N II] line ratio versus CO $J(4 \rightarrow 3)/CI(1 \rightarrow 0)$ (a dense to total molecular gas mass tracer) for a range of sources ([Wright et al. 1991](#); [Petuchowski et al. 1994](#); [Zhang et al. 2001](#); [Oberst et al. 2006](#); [Rigopoulou et al. 2013](#); [Rosenberg et al. 2014, 2015](#); [Zhao et al. 2016](#)).

Using our measurements of the line intensities, we find an electron density of $n_e = 290^{+90}_{-70} \text{cm}^{-3}$. This elevated electron density could explain the discrepancy found between the [N II] 205 μm and L_{IR} -derived SFRs by [Harrington et al. \(2019\)](#), since in that work a low electron density — $n_e \approx 30 \text{cm}^{-3}$ — was assumed.

There may be a potential bias in our measurement if the local radiation field is so intense that optical pumping of [N II] provides a significant contribution to the excitation ([Flannery et al. 1979](#)). We can test if this is likely to be important by comparing the pumping collision rate with the inferred collision rate from our data. The pump rate can be expressed as $R_p = 1835\nu U_\nu$, where νU_ν is a measure of the strength of the radiation field in erg cm^{-3} . In the Solar neighbourhood, $\nu U_\nu \approx 7 \times 10^{-14} \text{erg cm}^{-3}$ at $\nu \approx 3 \times 10^{15} \text{Hz}$ corresponding to the $^3D_1 \rightarrow ^3P_0$ transition ([Draine 2011](#)). The interstellar UV radiation field in galaxies like 9109 is not well constrained, however [Danielson et al. \(2011\)](#) found for the Cosmic Eyelash that the cold gas was exposed to a UV radiation field that is roughly 1000 \times that of the local Galactic ISM. If we assume similar conditions for 9109, then we obtain a pump rate of $R_p \approx 10^{-7} \text{s}^{-1}$, or approximately 2 per cent of the collision rate. Thus, even with rather extreme local radiation fields — perhaps only relevant for the gas in the immediate vicinity of O and B stars — pumping has a negligible impact on the [N II] excitation.

4. INTERPRETATION AND DISCUSSION

Recent studies of electron densities in the ISM of star-forming galaxies at high redshift using optical/near-infrared (NIR) tracers of n_e — such as O II and S II — have also found values significantly higher than those typically ob-

served in the local Universe, with $n_e \gtrsim 100 \text{ cm}^{-3}$ not uncommon in samples of ($\text{H}\alpha$ -selected) star-forming galaxies with $\text{SFR} \sim 1\text{--}100 \text{ s M}_\odot \text{ yr}^{-1}$ (Masters et al. 2014; Shirazi et al. 2014). Kaasinen et al. (2017) connected these elevated electron densities to the high SFRs observed in galaxies at $z \sim 1\text{--}2$, pointing out that the average electron densities in their high-redshift and local samples are comparable, when controlled for SFR. Shimakawa et al. (2015) and Jiang et al. (2019) note a correlation between the surface density of star formation (Σ_{SFR}) and n_e , providing further evidence of the close relationship between star formation and ionised ISM density. This is not surprising, since if star formation depends on the density distribution of the cold ISM, and Σ_{SFR} is enhanced when a large fraction of the molecular ISM is driven to high density, then that will likely be reflected in the resultant ionised phase density in the vicinity of those star-forming regions.

The integrated profiles of both [N II] lines resemble the integrated CO $J(4\rightarrow 3)$ and C I (1–0) line profiles (recall Fig. 2), indicating that the ionised and molecular tracers originate from the same material and local environments. Geach et al. (2018) modelled the CO $J(4\rightarrow 3)$ emission with a rotating disk motivated by the dynamics of circumnuclear gas seen in local ULIRGs (Downes & Solomon 1998), and this provided an excellent fit to the data, with properties similar to another strongly lensed system, SDP 81 (e.g. ALMA Partnership et al. 2015; Swinbank et al. 2015; Dye et al. 2015; Hatsukade et al. 2015; Rybak et al. 2020). It is reasonable to assume that the [N II] emission is tracing the ionised component of the ISM across the same disk, and is broadly co-spatial with the star-forming molecular gas. The measured electron density of $n_e = 290^{+90}_{-70} \text{ cm}^{-3}$ is significantly higher than that expected for the WIM, which is comprised of material at densities 3–4 orders of magnitude lower (Gaensler et al. 2008; Weisberg et al. 2008).

The electron density in 9io9 is high, but not extreme when we consider individual local star-forming environments. For example, the Galactic H II region, G333.6–0.2, has an electron density, $\approx 300 \text{ cm}^{-3}$, also determined via the [N II] ratio (Colgan et al. 1993). This is consistent with the conditions in 9io9, with the key difference that we are measuring the characteristic electron density on scales of several kiloparsecs, rather than for an individual star-forming complex. Thus, a possible scenario is that star formation in 9io9 is proceeding in environments that resemble ‘normal’ star-forming regions like G333.6–0.2 but with the key distinction that, while G333.6–0.2 represents a tiny fraction of the total Milky Way ISM by mass and volume, in 9io9 the *majority* of the ISM may be in this state.

There is support for this ‘globally dense’ picture in the molecular phase tracers. Papadopoulos & Geach (2012) argue that the CO $J(4\rightarrow 3)$ /C I (1–0) ratio is an excellent empir-

ical tracer of the ratio of dense, actively star-forming molecular gas to the total molecular reservoir. Geach et al. (2018) show that the observed ratio in 9io9 is consistent with over half of the molecular ISM having been driven to high density. It follows that the H II regions produced by massive star formation should have correspondingly elevated electron densities. Hints of this link can be seen in Fig. 4, where we compare the CO $J(4\rightarrow 3)$ /C I (1–0) ratio to the [N II] line ratio for 9io9 and a sample of sources from the literature spanning a range of densities. Generally, there is a weak trend that galaxies or regions with high electron densities — as traced by the [N II] line ratio — have a correspondingly high dense molecular gas fraction — as traced by the CO $J(4\rightarrow 3)$ /C I (1–0) ratio.

Given 9io9’s clear disk-like structure, most evident in the shape of the line profiles and confirmed by the excellent fits achieved for disk- or ring-like kinematic models (Geach et al. 2018), we can consider a detailed picture of star formation in this galaxy. A plausible scenario is that the disk comprises an ensemble of dense clumps containing a large fraction of the total ISM, within which star formation occurs. This is not a novel concept, of course. Early work with *Hubble Space Telescope* suggested that a large fraction of star formation in high-redshift Lyman-break galaxies may occur in large blue clumps, on scales of up to 1 kpc (e.g. Cowie et al. 1995; Elmegreen et al. 2005). More recently, resolved imaging of strongly lensed dusty star-forming systems suggests the presence of distinct regions of embedded high-density star formation on scales of $\sim 100 \text{ pc}$, with luminosity densities comparable to the cores of local giant molecular clouds (e.g. Swinbank et al. 2010, 2015; Hatsukade et al. 2015, though see Ivison et al. 2020). This led to a ‘giant clump’ model of star formation in the most vigorously star-forming galaxies at high redshift, where the 100 pc-scale clumps thought to be present in objects like the Cosmic Eyelash resemble scaled-up versions of the dense, 1 pc-scale cores within local giant molecular clouds.

The physical argument put forward to explain the formation of such structures is through disk instabilities, which conveniently circumvents the requirement for mergers or interactions to drive gas to high densities, although interactions are known to be common — perhaps even ubiquitous — amongst SMGs (e.g. Engel et al. 2010). At high gas fractions and surface densities, disks will be Toomre-unstable and undergo local collapse (Toomre 1964; Noguchi 1999; Dekel et al. 2009). The Jeans length scale on which this fragmentation occurs for the typical gas densities and velocity dispersions *inferred* in objects like the Cosmic Eyelash, SDP 81 and 9io9 is broadly consistent with the $\approx 100 \text{ pc}$ clump scales described above (e.g. Swinbank et al. 2015; Hatsukade et al.

2015)². The current source plane resolution in 9io9 is around 300 pc and so we cannot yet address this question; however, the brightness of the target (approaching 1 Jy) makes it a prime candidate for pushing to very long baselines to resolve the disk sub-structure, allowing us to link the physical conditions of the ISM explored here on global scales to the spatial distribution of the gas down to 10s of parsecs.

5. CONCLUSIONS

We have reported new ALMA Band 8 and 9 observations of a strongly lensed HyLIRG at $z = 2.6$, targeting the [N II] fine-structure line emission and thermal continuum in the rest-frame far-infrared waveband. Our main findings are as follows:

- We report detections of both the 122- and 205- μm [N II] emission lines, which trace the ionised ISM. The [N II] lines match the double-horned line profiles seen in CO $J(4\rightarrow 3)$ and C I (1–0), reported by Geach et al. (2018) and well-modelled by a rotating disk. This implies that the ionised gas is broadly co-located with the molecular material on scales of several kiloparsecs.
- We use the 122/205 μm line ratio to estimate the average electron density in the ISM, finding $n_e \approx 300 \text{ cm}^{-3}$, an order of magnitude above that of the (average) Milky Way, comparable with measurements of the electron density in discrete Galactic star-forming environments.
- We demonstrate a tentative (but expected) trend between the ratio of dense molecular gas and the total molecular gas reservoir, as traced by CO $J(4\rightarrow 3)$ and C I (1–0), and the [N II] line ratio. If the former

is a tracer of the dense molecular gas fraction as Papadopoulos & Geach (2012) argue, then the correlation with the [N II] ratio and therefore ionised gas density reveals a picture of ‘globally dense’ ISM, where a significant fraction of the molecular component has been driven to high density — possibly through violent disk instabilities, with or without galaxy interactions — with myriad individual H II regions dominating the observed [N II] emission.

9io9 is a remarkably extreme system, fortuitously lensed to provide us a glimpse of its inner workings. Our findings support a picture where the nature of star formation in this galaxy might not necessarily differ from the conditions of star formation in our own Milky Way. The key difference is that a far higher fraction of the ISM is currently participating in that star formation.

ACKNOWLEDGEMENTS

M.J.D. and J.E.G. are supported by the Royal Society. S.D. is supported by an STFC Rutherford Fellowship. This paper makes use of the following ALMA data: ADS/JAO.ALMA#2017.1.00814.S. ALMA is a partnership of ESO (representing its member states), NSF (USA) and NINS (Japan), together with NRC (Canada), MOST and ASIAA (Taiwan), and KASI (Republic of Korea), in cooperation with the Republic of Chile. The Joint ALMA Observatory is operated by ESO, AUI/NRAO and NAOJ. Funded by the Deutsche Forschungsgemeinschaft (DFG, German Research Foundation) under Germany’s Excellence Strategy — EXC-2094 — 390783311. This research has made use of the University of Hertfordshire high-performance computing facility (<http://stri-cluster.herts.ac.uk>).

REFERENCES

- ALMA Partnership, Vlahakis, C., Hunter, T. R., et al. 2015, *ApJL*, 808, L4, doi: [10.1088/2041-8205/808/1/L4](https://doi.org/10.1088/2041-8205/808/1/L4)
- Barger, A. J., Cowie, L. L., Sanders, D. B., et al. 1998, *Nature*, 394, 248, doi: [10.1038/28338](https://doi.org/10.1038/28338)
- Brown, T., & Wilson, C. D. 2019, *The Astrophysical Journal*, 879, 17, doi: [10.3847/1538-4357/ab2246](https://doi.org/10.3847/1538-4357/ab2246)
- Colgan, S. W. J., Haas, M. R., Erickson, E. F., et al. 1993, *The Astrophysical Journal*, 413, 237, doi: [10.1086/172991](https://doi.org/10.1086/172991)
- Conley, A., Cooray, A., Vieira, J. D., et al. 2011, *The Astrophysical Journal*, 732, L35, doi: [10.1088/2041-8205/732/2/L35](https://doi.org/10.1088/2041-8205/732/2/L35)
- Cowie, L. L., Hu, E. M., & Songaila, A. 1995, *The Astronomical Journal*, 110, 1576, doi: [10.1086/117631](https://doi.org/10.1086/117631)
- Danielson, A. L. R., Swinbank, A. M., Smail, I., et al. 2011, *Monthly Notices of the Royal Astronomical Society*, 410, 1687, doi: [10.1111/j.1365-2966.2010.17549.x](https://doi.org/10.1111/j.1365-2966.2010.17549.x)
- Danielson, A. L. R., Swinbank, A. M., Smail, I., et al. 2013, *MNRAS*, 436, 2793, doi: [10.1093/mnras/stt1775](https://doi.org/10.1093/mnras/stt1775)
- Davies, R. I., Sternberg, A., Lehnert, M., & Tacconi-Garman, L. E. 2003, *The Astrophysical Journal*, 597, 907, doi: [10.1086/378634](https://doi.org/10.1086/378634)
- Dekel, A., Sari, R., & Ceverino, D. 2009, *The Astrophysical Journal*, 703, 785, doi: [10.1088/0004-637X/703/1/785](https://doi.org/10.1088/0004-637X/703/1/785)
- Dessauges-Zavadsky, M., Richard, J., Combes, F., et al. 2019, *Nature Astronomy*, 3, 1115, doi: [10.1038/s41550-019-0874-0](https://doi.org/10.1038/s41550-019-0874-0)
- Downes, D., & Solomon, P. M. 1998, *The Astrophysical Journal*, 507, 615, doi: [10.1086/306339](https://doi.org/10.1086/306339)

² Note that in the case of the Cosmic Eyelash Ivison et al. (2020) have shown these clumps to be spurious — the result of over-cleaning a low-signal-to-noise interferometric image.

- Draine, B. T. 2011, *Physics of the Interstellar and Intergalactic Medium* (Princeton University Press)
- Dye, S., Furlanetto, C., Swinbank, A. M., et al. 2015, *Monthly Notices of the Royal Astronomical Society*, 452, 2258, doi: [10.1093/mnras/stv1442](https://doi.org/10.1093/mnras/stv1442)
- Dye, S., Furlanetto, C., Swinbank, A. M., et al. 2015, *MNRAS*, 452, 2258, doi: [10.1093/mnras/stv1442](https://doi.org/10.1093/mnras/stv1442)
- Dye, S., Furlanetto, C., Dunne, L., et al. 2018, *Monthly Notices of the Royal Astronomical Society*, 476, 4383, doi: [10.1093/mnras/sty513](https://doi.org/10.1093/mnras/sty513)
- Elmegreen, D. M., Elmegreen, B. G., Rubin, D. S., & Schaffer, M. A. 2005, *The Astrophysical Journal*, 631, 85, doi: [10.1086/432502](https://doi.org/10.1086/432502)
- Engel, H., Tacconi, L. J., Davies, R. I., et al. 2010, *ApJ*, 724, 233, doi: [10.1088/0004-637X/724/1/233](https://doi.org/10.1088/0004-637X/724/1/233)
- Flannery, B. P., Rybicki, G. B., & Sarazin, C. L. 1979, *The Astrophysical Journal*, 229, 1057, doi: [10.1086/157040](https://doi.org/10.1086/157040)
- Gaensler, B. M., Madsen, G. J., Chatterjee, S., & Mao, S. A. 2008, *Publications of the Astronomical Society of Australia*, 25, 184, doi: [10.1071/AS08004](https://doi.org/10.1071/AS08004)
- Gao, Y., & Solomon, P. M. 2004, *ApJ*, 606, 271, doi: [10.1086/382999](https://doi.org/10.1086/382999)
- Geach, J. E., Ivison, R. J., Dye, S., & Oteo, I. 2018, *The Astrophysical Journal*, 866, L12, doi: [10.3847/2041-8213/aae375](https://doi.org/10.3847/2041-8213/aae375)
- Geach, J. E., More, A., Verma, A., et al. 2015, *Monthly Notices of the Royal Astronomical Society*, 452, 502, doi: [10.1093/mnras/stv1243](https://doi.org/10.1093/mnras/stv1243)
- George, R. D., Ivison, R. J., Smail, I., et al. 2014, *MNRAS*, 442, 1877, doi: [10.1093/mnras/stu967](https://doi.org/10.1093/mnras/stu967)
- Goldsmith, P. F., Yıldız, U. A., Langer, W. D., & Pineda, J. L. 2015, *The Astrophysical Journal*, 814, 133, doi: [10.1088/0004-637X/814/2/133](https://doi.org/10.1088/0004-637X/814/2/133)
- Harrington, K. C., Yun, M. S., Cybulski, R., et al. 2016, *Monthly Notices of the Royal Astronomical Society*, 458, 4383, doi: [10.1093/mnras/stw614](https://doi.org/10.1093/mnras/stw614)
- Harrington, K. C., Vishwas, A., Weiß, A., et al. 2019, *Monthly Notices of the Royal Astronomical Society*, 488, 1489, doi: [10.1093/mnras/stz1740](https://doi.org/10.1093/mnras/stz1740)
- Hatsukade, B., Tamura, Y., Iono, D., et al. 2015, *Publications of the Astronomical Society of Japan*, 67, doi: [10.1093/pasj/psv061](https://doi.org/10.1093/pasj/psv061)
- Herrera-Camus, R., Bolatto, A., Smith, J. D., et al. 2016, *The Astrophysical Journal*, 826, 175, doi: [10.3847/0004-637X/826/2/175](https://doi.org/10.3847/0004-637X/826/2/175)
- Hodge, J. A., & da Cunha, E. 2020, arXiv:2004.00934 [astro-ph]. <http://arxiv.org/abs/2004.00934>
- Hughes, D. H., Serjeant, S., Dunlop, J., et al. 1998, *Nature*, 394, 241, doi: [10.1038/28328](https://doi.org/10.1038/28328)
- Ivison, R. J., Page, M. J., Cirasuolo, M., et al. 2019, *MNRAS*, 489, 427, doi: [10.1093/mnras/stz2180](https://doi.org/10.1093/mnras/stz2180)
- Ivison, R. J., Papadopoulos, P. P., Smail, I., et al. 2011, *Monthly Notices of the Royal Astronomical Society*, 412, 1913, doi: [10.1111/j.1365-2966.2010.18028.x](https://doi.org/10.1111/j.1365-2966.2010.18028.x)
- Ivison, R. J., Richard, J., Biggs, A. D., et al. 2020, *Monthly Notices of the Royal Astronomical Society: Letters*, 495, L1, doi: [10.1093/mnras/slaa046](https://doi.org/10.1093/mnras/slaa046)
- Ivison, R. J., Swinbank, A. M., Swinyard, B., et al. 2010, *Astronomy and Astrophysics*, 518, L35, doi: [10.1051/0004-6361/201014548](https://doi.org/10.1051/0004-6361/201014548)
- Jiang, T., Malhotra, S., Yang, H., & Rhoads, J. E. 2019, *The Astrophysical Journal*, 872, 146, doi: [10.3847/1538-4357/aace79](https://doi.org/10.3847/1538-4357/aace79)
- Kaasinen, M., Bian, F., Groves, B., Kewley, L., & Gupta, A. 2017, *Monthly Notices of the Royal Astronomical Society*, 465, 3220, doi: [10.1093/mnras/stw2827](https://doi.org/10.1093/mnras/stw2827)
- Koopmans, L. V. E., Treu, T., Bolton, A. S., Burles, S., & Moustakas, L. A. 2006, *The Astrophysical Journal*, 649, 599, doi: [10.1086/505696](https://doi.org/10.1086/505696)
- Marshall, P. J., Verma, A., More, A., et al. 2016, *Monthly Notices of the Royal Astronomical Society*, 455, 1171, doi: [10.1093/mnras/stv2009](https://doi.org/10.1093/mnras/stv2009)
- Masters, D., McCarthy, P., Siana, B., et al. 2014, *The Astrophysical Journal*, 785, 153, doi: [10.1088/0004-637X/785/2/153](https://doi.org/10.1088/0004-637X/785/2/153)
- Menéndez-Delmestre, K., Blain, A. W., Smail, I., et al. 2009, *The Astrophysical Journal*, 699, 667, doi: [10.1088/0004-637X/699/1/667](https://doi.org/10.1088/0004-637X/699/1/667)
- More, A., Verma, A., Marshall, P. J., et al. 2016, *Monthly Notices of the Royal Astronomical Society*, 455, 1191, doi: [10.1093/mnras/stv1965](https://doi.org/10.1093/mnras/stv1965)
- Motte, F., Nony, T., Louvet, F., et al. 2018, *Nature Astronomy*, 2, 478, doi: [10.1038/s41550-018-0452-x](https://doi.org/10.1038/s41550-018-0452-x)
- Noguchi, M. 1999, *The Astrophysical Journal*, 514, 77, doi: [10.1086/306932](https://doi.org/10.1086/306932)
- Oberst, T. E., Parshley, S. C., Stacey, G. J., et al. 2006, *The Astrophysical Journal*, 652, L125, doi: [10.1086/510289](https://doi.org/10.1086/510289)
- Oteo, I., Zhang, Z.-Y., Yang, C., et al. 2017, *The Astrophysical Journal*, 850, 170, doi: [10.3847/1538-4357/aa8ee3](https://doi.org/10.3847/1538-4357/aa8ee3)
- Papadopoulos, P. P., & Geach, J. E. 2012, *The Astrophysical Journal*, 757, 157, doi: [10.1088/0004-637X/757/2/157](https://doi.org/10.1088/0004-637X/757/2/157)
- Petuchowski, S. J., Bennett, C. L., Haas, M. R., et al. 1994, *The Astrophysical Journal Letters*, 427, L17, doi: [10.1086/187354](https://doi.org/10.1086/187354)
- Planck Collaboration, Ade, P. A. R., Aghanim, N., et al. 2016, *Astronomy and Astrophysics*, 594, A13, doi: [10.1051/0004-6361/201525830](https://doi.org/10.1051/0004-6361/201525830)
- Riechers, D. A., Hodge, J., Walter, F., Carilli, C. L., & Bertoldi, F. 2011, *The Astrophysical Journal*, 739, L31, doi: [10.1088/2041-8205/739/1/L31](https://doi.org/10.1088/2041-8205/739/1/L31)
- Rigopoulou, D., Hurley, P. D., Swinyard, B. M., et al. 2013, *Monthly Notices of the Royal Astronomical Society*, 434, 2051, doi: [10.1093/mnras/stt1149](https://doi.org/10.1093/mnras/stt1149)

- Romano, D., Matteucci, F., Zhang, Z.-Y., Ivison, R. J., & Ventura, P. 2019, *MNRAS*, 490, 2838, doi: [10.1093/mnras/stz2741](https://doi.org/10.1093/mnras/stz2741)
- Romano, D., Matteucci, F., Zhang, Z.-Y., Papadopoulos, P. P., & Ivison, R. J. 2017, *Monthly Notices of the Royal Astronomical Society*, 470, 401, doi: [10.1093/mnras/stx1197](https://doi.org/10.1093/mnras/stx1197)
- Rosenberg, M. J. F., Kazandjian, M. V., van der Werf, P. P., et al. 2014, *Astronomy & Astrophysics*, 564, A126, doi: [10.1051/0004-6361/201323109](https://doi.org/10.1051/0004-6361/201323109)
- Rosenberg, M. J. F., Werf, P. P. v. d., Aalto, S., et al. 2015, *The Astrophysical Journal*, 801, 72, doi: [10.1088/0004-637X/801/2/72](https://doi.org/10.1088/0004-637X/801/2/72)
- Rybak, M., Hodge, J. A., Vegetti, S., et al. 2020, *Monthly Notices of the Royal Astronomical Society*, 494, 5542, doi: [10.1093/mnras/staa879](https://doi.org/10.1093/mnras/staa879)
- Schneider, F. R. N., Sana, H., Evans, C. J., et al. 2018, *Science*, 359, 69, doi: [10.1126/science.aan0106](https://doi.org/10.1126/science.aan0106)
- Schneider, P., & Sluse, D. 2013, *Astronomy & Astrophysics*, 559, A37, doi: [10.1051/0004-6361/201321882](https://doi.org/10.1051/0004-6361/201321882)
- Shimakawa, R., Kodama, T., Steidel, C. C., et al. 2015, *Monthly Notices of the Royal Astronomical Society*, 451, 1284, doi: [10.1093/mnras/stv915](https://doi.org/10.1093/mnras/stv915)
- Shirazi, M., Brinchmann, J., & Rahmati, A. 2014, *The Astrophysical Journal*, 787, 120, doi: [10.1088/0004-637X/787/2/120](https://doi.org/10.1088/0004-637X/787/2/120)
- Simpson, J. M., Swinbank, A. M., Smail, I., et al. 2014, *The Astrophysical Journal*, 788, 125, doi: [10.1088/0004-637X/788/2/125](https://doi.org/10.1088/0004-637X/788/2/125)
- Smail, I., Ivison, R. J., & Blain, A. W. 1997, *The Astrophysical Journal Letters*, 490, L5, doi: [10.1086/311017](https://doi.org/10.1086/311017)
- Solomon, P. M., Downes, D., Radford, S. J. E., & Barrett, J. W. 1997, *The Astrophysical Journal*, 478, 144, doi: [10.1086/303765](https://doi.org/10.1086/303765)
- Su, T., Marriage, T. A., Asboth, V., et al. 2017, *Monthly Notices of the Royal Astronomical Society*, 464, 968, doi: [10.1093/mnras/stw2334](https://doi.org/10.1093/mnras/stw2334)
- Swinbank, A. M., Smail, I., Longmore, S., et al. 2010, *Nature*, 464, 733, doi: [10.1038/nature08880](https://doi.org/10.1038/nature08880)
- Swinbank, A. M., Dye, S., Nightingale, J. W., et al. 2015, *The Astrophysical Journal*, 806, L17, doi: [10.1088/2041-8205/806/1/L17](https://doi.org/10.1088/2041-8205/806/1/L17)
- Tayal, S. S. 2011, *The Astrophysical Journal Supplement Series*, 195, 12, doi: [10.1088/0067-0049/195/2/12](https://doi.org/10.1088/0067-0049/195/2/12)
- Thomson, A. P., Ivison, R. J., Smail, I., et al. 2012, *MNRAS*, 425, 2203, doi: [10.1111/j.1365-2966.2012.21584.x](https://doi.org/10.1111/j.1365-2966.2012.21584.x)
- Toft, S., Smolčić, V., Magnelli, B., et al. 2014, *The Astrophysical Journal*, 782, 68, doi: [10.1088/0004-637X/782/2/68](https://doi.org/10.1088/0004-637X/782/2/68)
- Toomre, A. 1964, *The Astrophysical Journal*, 139, 1217, doi: [10.1086/147861](https://doi.org/10.1086/147861)
- Viero, M. P., Asboth, V., Roseboom, I. G., et al. 2014, *The Astrophysical Journal Supplement Series*, 210, 22, doi: [10.1088/0067-0049/210/2/22](https://doi.org/10.1088/0067-0049/210/2/22)
- Wardlow, J. L., Cooray, A., De Bernardis, F., et al. 2013, *The Astrophysical Journal*, 762, 59, doi: [10.1088/0004-637X/762/1/59](https://doi.org/10.1088/0004-637X/762/1/59)
- Warren, S. J., & Dye, S. 2003, *The Astrophysical Journal*, 590, 673, doi: [10.1086/375132](https://doi.org/10.1086/375132)
- Weisberg, J. M., Stanimirović, S., Xilouris, K., et al. 2008, *The Astrophysical Journal*, 674, 286, doi: [10.1086/523345](https://doi.org/10.1086/523345)
- Wright, E. L., Mather, J. C., Bennett, C. L., et al. 1991, *The Astrophysical Journal*, 381, 200, doi: [10.1086/170641](https://doi.org/10.1086/170641)
- Zhang, X., Lee, Y., Bolatto, A., & Stark, A. A. 2001, *The Astrophysical Journal*, 553, 274, doi: [10.1086/320628](https://doi.org/10.1086/320628)
- Zhang, Z.-Y., Romano, D., Ivison, R. J., Papadopoulos, P. P., & Matteucci, F. 2018, *Nature*, 558, 260, doi: [10.1038/s41586-018-0196-x](https://doi.org/10.1038/s41586-018-0196-x)
- Zhang, Z.-Y., Ivison, R. J., George, R. D., et al. 2018, *MNRAS*, 481, 59, doi: [10.1093/mnras/sty2082](https://doi.org/10.1093/mnras/sty2082)
- Zhao, Y., Lu, N., Xu, C. K., et al. 2016, *The Astrophysical Journal*, 819, 69, doi: [10.3847/0004-637X/819/1/69](https://doi.org/10.3847/0004-637X/819/1/69)